Benchmark Cases for Galloping with Results Obtained from Wind Tunnel Facilities—Validation of a Finite Element Model

Renaud Keutgen and Jean-Louis Lilien

Abstract—**The full set of data of recent galloping results obtained from wind tunnel facilities are presented. These results allow to define benchmark cases for the validation of any numerical model of galloping. This validation is realized in this paper with a finite element model.**

I. Introduction

GALLOPING or the large vibrations of overhead transmission lines due to wind action and to the presence of an ice deposit on the conductors is a repetitive problem for badly situated lines. As the phenomenon has been observed for many years, correlations between line design parameters and the shape or the amplitude of the vibration have been found [1]. This is a statistical point of view, although it requires a good physical knowledge of the phenomenon in order to find significant variables for the correlations. Another approach consists of modeling the line, the wind and the ice deposit in order to assess, by simulation on a computer, the amplitude and the shape of the vibration and the efficiency of protection systems. This approach is complementary to the previous one; it allows confirmation of certain tendencies and then to continue the analysis for a particular design parameter by repetitive simulations with different values of this parameter. Nevertheless, to have confidence in such simulations, the numerical model needs first to be validated. There exists on this point a considerable lack in the galloping literature. There are numerous numerical models of galloping but very few benchmark cases for their validation.

In this paper, we present galloping results obtained from wind tunnel facilities by O. Chabart *et al.* [2]. These wind tunnel measurements are exceptional because this is the first time that a full experimental set of data of galloping instabilities is published. To realize these measurements, O. Chabart *et al.* have decided to experiment on a string suspended model of a cable sample on which the ice deposit has been modeled with silicone. Several aspects of a real line are not reproduced, such as the tension variations in the cable or the complexity of the bundle torsional stiffness. However, appropriate ratios between the fundamental frequencies (vertical, rotational, transversal) are chosen to observe Den-Hartog [3] as well as flutter galloping instabilities [4].

The quasisteady aerodynamic coefficients (drag, lift, moment) have been measured for a fixed cable sample and then the fixations have been removed to measure the galloping amplitudes.

We further introduce a finite element model which is able to simulate these experimental conditions. As all the galloping models, this finite element modeling is based on the assumption that, in galloping conditions, the action of the aerodynamic forces is quasisteady. We thus have here the opportunity to check this hypothesis for different kind of instabilities.

In the last section of this paper, we realize this validation process by comparisons between the experimental and the simulated results.

II. Wind Tunnel Experimental Data

In this section, we provide the full set of data of the wind tunnel mounting realized by O. Chabart *et al.* [2]. They will serve to define three benchmark cases that can be used to validate any numerical model of galloping. More details concerning the experimental procedure can be obtained in the above mentioned reference.

A. Conductor and Artificial Ice

The diameter of the conductor (used in Belgium for the 400 kV network) is 32.5 mm and the cross section is 620 mm^2. The outside layer of the conductor has been put on an aluminum tube of appropriate diameter in order to maintain a straight line of approximately 1 m sample (see Figs. 1 and 2).

Artificial ice has been chosen close to M. Tunstall's shape #1 [5] and adapted to the outside diameter of the conductor. The "ice" in silicone (density 1.13) has been modeled on the cable with a wooden mold on which the roughness pattern has been printed (see Fig. 2). This pattern has been copied from the original sample (itself obtained from a sample of real ice

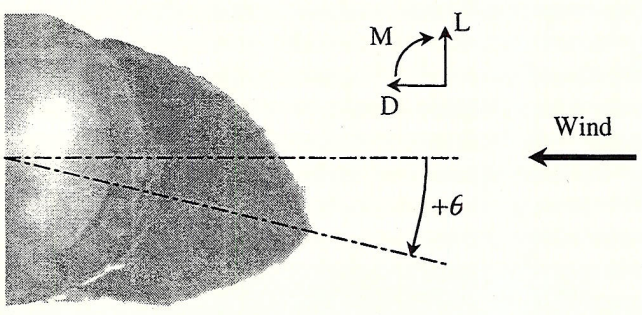

Fig. 1. Artificial ice on the conductor—conventions.

Manuscript received July 27, 1998; revised January 8, 1999.

The authors are with the Montefiore Electrical Institute, University of Liège, B-4000 Liège, Belgium.

Publisher Item Identifier S 0885-8977(00)00661-0.

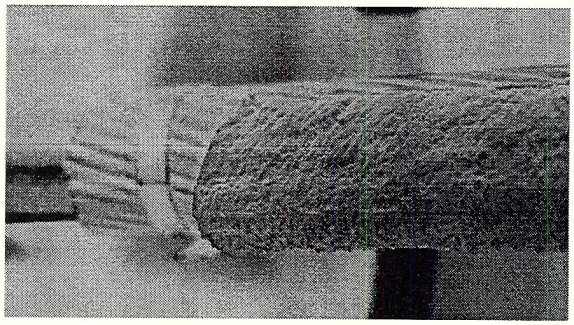

Fig. 2. Aluminum tube, outside layer of the conductor, and artificial ice.

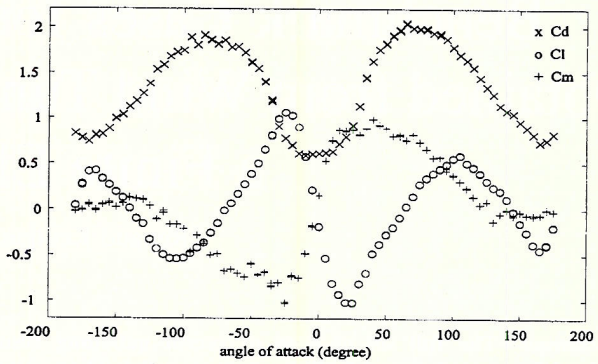

Fig. 3. Quasisteady measured aerodynamic coefficients of drag (Cd), lift (Cl) and moment (Cm).

accretion). The length of the artificial ice is 0.8 in (see Fig. 5) and its eccentricity, i.e., the ratio between the ice thickness and the radius of the conductor is 1.32. The distance between the center of gravity of the ice and the center of the cable is 2.17×10^{-2} m.

The quasisteady measured coefficients of drag, lift and moment as functions of the angle of attack (convention of Fig. 1) are shown in Fig. 3. These experimental points are practically independent of the wind speed. Fourier's interpolations of these three experimental curves are provided in the Appendix.

B. Structural Data

The test sample is suspended by four vertical springs which are prestressed in order to limit the static deformation due to the weight of the structure (see Fig. 4). The prestress is equal to 3.5 N for each vertical spring while their stiffness is equal to 14 N/m.

A plan view of the mounting is provided on Fig. 5. This is an assembly of tubes (see view A–A and B–B for their characteristics), vertical and horizontal springs and different joints (noted with the letters a, b, c, d, e, and f on Fig. 5) which allow connection of the different elements. The vertical springs are attached to the structure at the joints marked with the letter b on Fig. 5. The horizontal springs have also a stiffness of 14 N/m and in the static equilibrium configuration (without wind) the tension in each horizontal spring is equal to 2.8 N.

Two vertical plates are placed just at the extremities of the ice sample to prevent the wind from blowing on the springs and the part of the structure without ice. Two circular openings in these plates (diameter 0.2 m) allow the movement of the sample but limit the maximum amplitude.

The minimum wind speed allowed by the wind tunnel is 8 m/s while the turbulence intensity is never above 1%.

The total weight of the structure is about 2.6 kg. The artificial ice weighs 0.446 kg. The equivalent volumetric mass of the outer layer of the conductor is 2229 kg/m^3 and the volumetric mass of the different aluminum tubes is 2700 kg/m^3.

The damping, measured by logarithmic decrement, is about 0.08% of the critical damping for the vertical and the transversal movements, and about 0.3% of the critical damping for the rotation.

C. Benchmark Cases

Two configurations characterized by a different ratio between the vertical and the torsional frequencies have been tested.

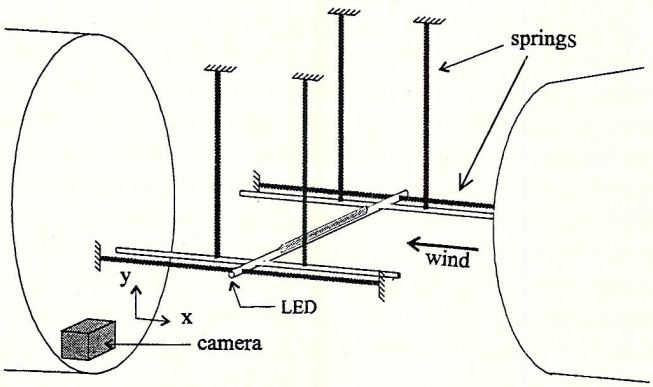

Fig. 4. String suspended mounting in the wind tunnel.

In the first configuration, the vertical springs have been placed at 0.12 m from the center of the test sample (see Fig. 5). For this configuration and without wind, the measured vertical, rotational and horizontal frequencies are, respectively, 0.845, 0.865, and 0.995 Hz, so that the ratio between the vertical and the torsional frequencies is about 1, as for a bundle conductor line. This coupling between the vertical and the torsional frequencies, which is a structural characteristic of bundle conductors, can lead to an aeroelastic instability of the system also called flutter galloping instability [4].

In the second configuration, the vertical springs have been placed at 0.36 m from the center of the test sample (see Fig. 5). In this case and without wind, the measured vertical, rotational and horizontal frequencies are respectively 0.85, 1.54, and 0.96 Hz, so that the ratio between the vertical and the torsional frequencies is about 0.5. This detuning between the vertical and the torsional frequencies is more typical of single conductor lines although in this case the ratio depends strongly on the position of ice and on the wind speed. For an accretion angle at $-180°$, the ratio is in any case even smaller (between 0.3 and 0.1) and galloping is then a pure aerodynamic instability which is predicted by Den-Hartog's criterion [3].

Den-Hartog's criterion applied to the aerodynamic curves of the test sample shows two unstable areas (between $-180°$ and $0°$), one is located around $-180°$ and the other one around $-35°$.

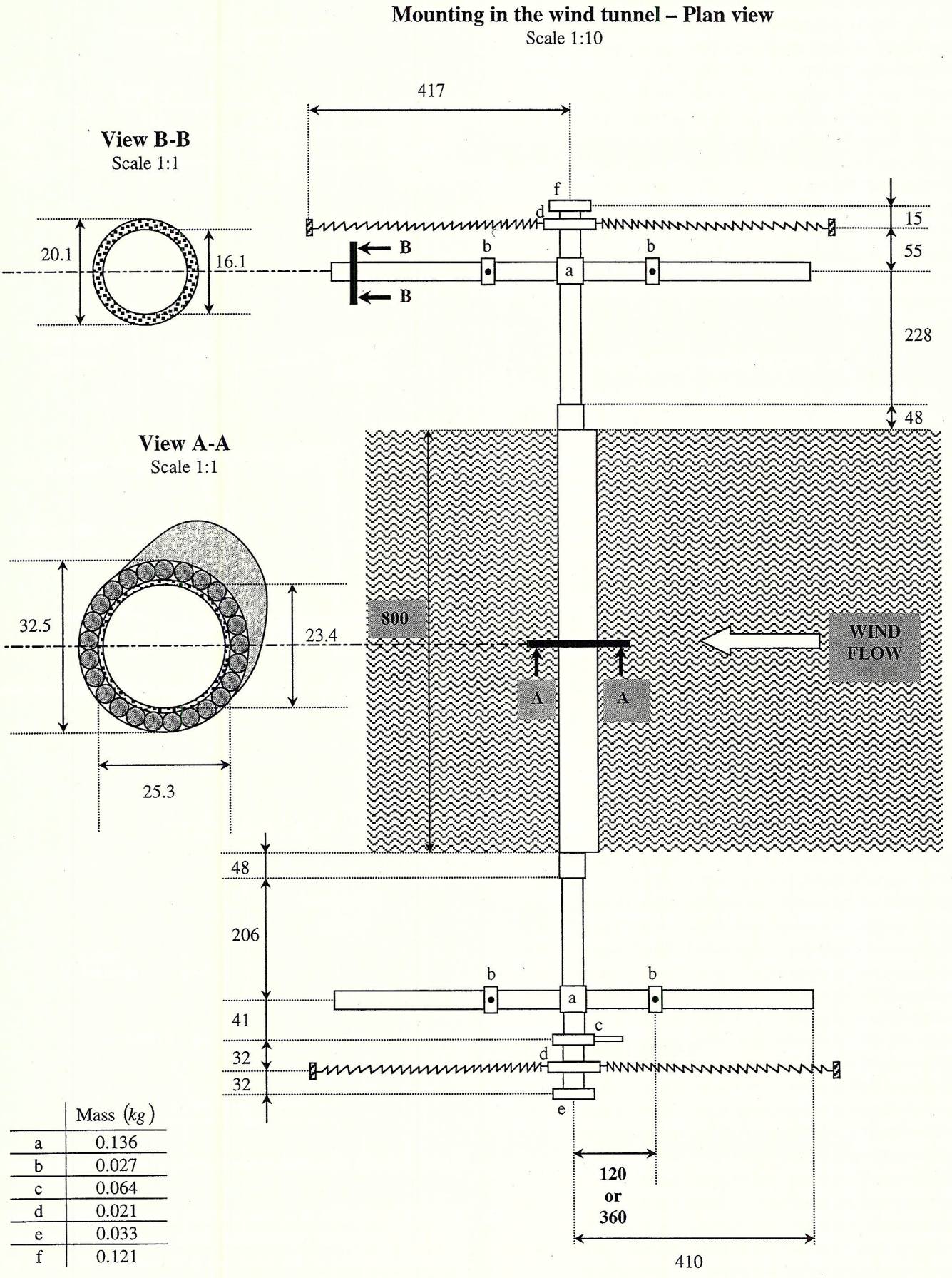

	Mass (kg)
a	0.136
b	0.027
c	0.064
d	0.021
e	0.033
f	0.121

Fig. 5. Technical representation of the suspended test sample. All the dimensions are in mm.

In the first configuration, two cases have been observed for which the peak-to-peak vertical amplitude was less than 0.2 m. The accretion angle and the wind speed corresponding to these cases are provided in Table I. The accretion angle θ, is the angle θ of Fig. 1 when the structure is horizontal. We will refer to these two cases with the abbreviations "Case_1a" and "Case_1b."

In the second configuration no galloping has been observed with a peak-to-peak vertical amplitude smaller than 0.2 m. Nevertheless, a reference case has been chosen to study the growth of the instability in Den-Hartog's only condition. The accretion angle and the wind speed corresponding to this case are provided in Table I. We will refer to this case with the abbreviation "Case_2."

TABLE I
PARAMETERS OF THE DIFFERENT BENCHMARK CASES

	f_v/f_θ	U_0 [m/s]	θ_i [deg]
Case_1a	0.98	9.7	-30
Case_1b	0.98	12	-165
Case_2	0.55	8.5	-180

III. FINITE ELEMENT MODELING

All the details of the mounting described above have been modeled with finite element software [6] (see Fig. 6).

The springs are represented by spring elements, the different tubes by beam elements, the joints by rigid elements and the characteristics of the artificial ice shape by a cable element with torsional degrees of freedom. For the aerodynamic properties of the ice shape, the aerodynamic curves given in the Appendix have been implemented in the cable element. Finally, the damping is modeled by a dashpot element.

A plan view of the finite element discretization is provide on Fig. 7.

Thanks to this finite element modeling we have created a numerical wind tunnel.

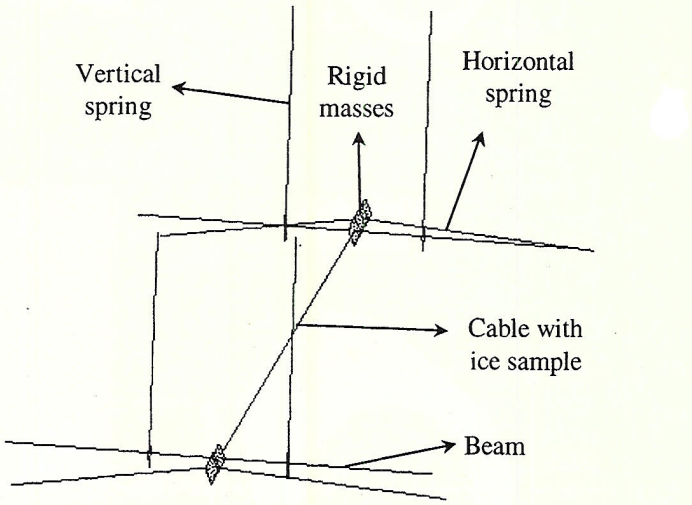

Fig. 6. Schematic view of the finite element modeling of the wind tunnel mounting.

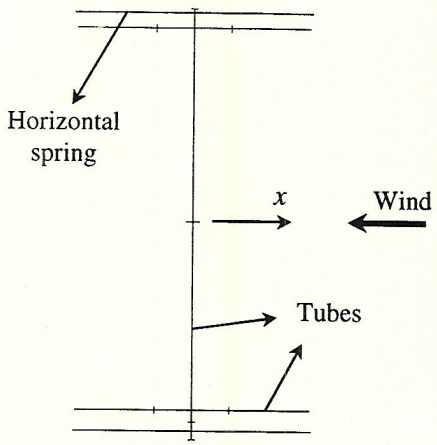

Fig. 7. Plan view of the finite element modeling of the wind tunnel mounting.

IV. VALIDATION

The comparisons between the experimental results and the simulated results are realized on Figs. 8 to 29 of the next pages. On the left column of each page we have plotted the experimental results and on the right column of each page we have plotted the corresponding simulated results.

In general the simulated results are in very good harmony with the experimental ones, and this for the galloping amplitudes and frequencies as well as for the phase lags.

In Case_la and Case_lb, we have in fact the combination of two instability mechanisms, as Den-Hartog's criterion is satisfied near $-30°$ and near $-165°$. For accretion angles between these two values, the test sample was also unstable without Den-Hartog's criterion, but the peak-to-peak galloping amplitudes exceeded 0.2 m (see Section II-B).

In Case_la, only the phase lag between the vertical and the torsional displacements is different for the experimental result and for the simulated result. No explanation was found about this difference.

In Case_lb and Case_2, we have not the time recording of the torsional behavior but only the final torsional amplitudes. In Case_lb the torsional amplitude was about $13°$ peak to peak for the experimental result as well as for the simulated result. In Case_2, the torsional amplitude was less than $3°$ peak to peak for both the experimental result and the simulated result. This difference between the torsional amplitudes of Case_lb and Case_2 has to be emphasized because it confirms that Den-Hartog's instability criterion is a pure vertical instability which doesn't need any dynamical contribution from the torsional movement (only the position of the accretion is important). In flutter galloping conditions the coupling between the vertical and the torsional movement is at the basis of the instability, so that the amplitude of the torsional movement is never negligible.

Wind tunnel measurements

Numerical wind tunnel simulations

Case_1a

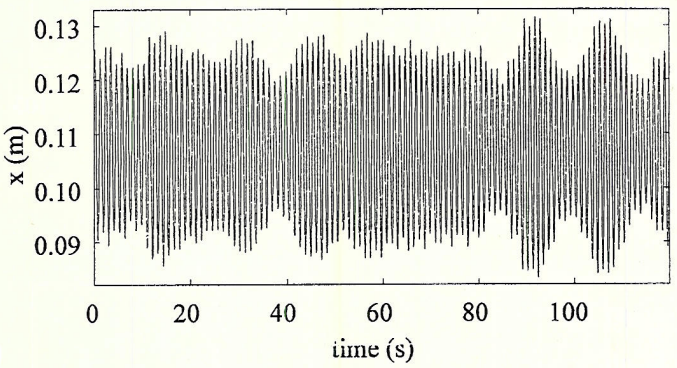

Fig. 8. Horizontal displacement, $U_0 = 9.7$ m/s, $\theta_i = -30°$.

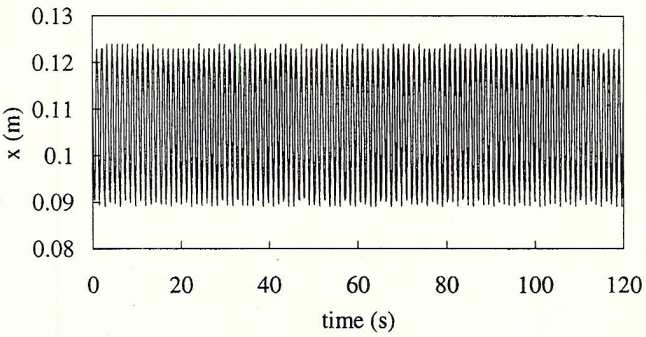

Fig. 9. Horizontal displacement, $U_0 = 9.7$ m/s, $\theta_i = -30°$.

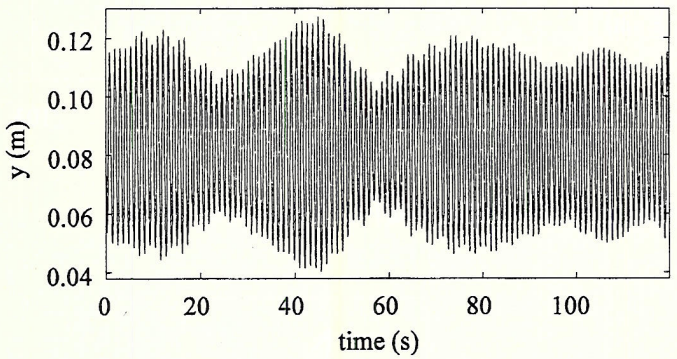

Fig. 10. Vertical displacement, $U_0 = 9.7$ m/s, $\theta_i = -30°$.

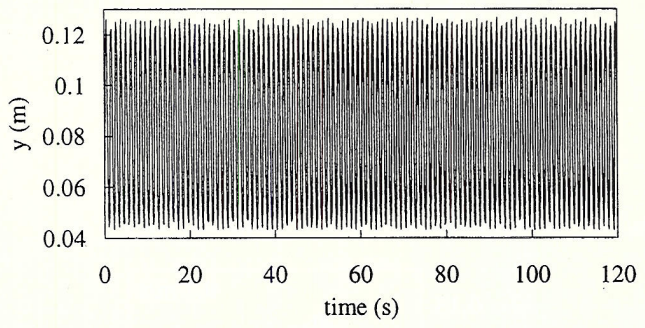

Fig. 11. Vertical displacement, $U_0 = 9.7$ m/s, $\theta_i = -30°$.

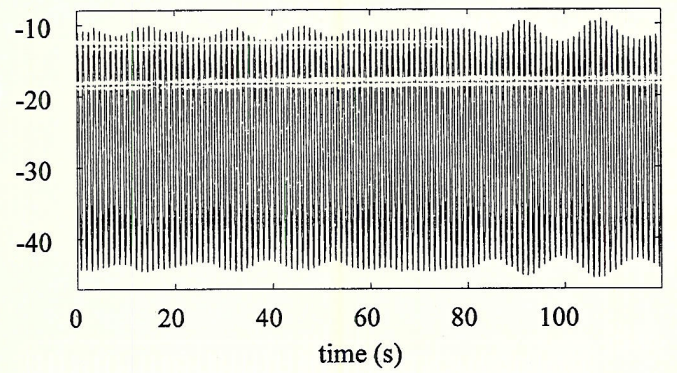

Fig. 12. Torsional displacement, $U_0 = 9.7$ m/s, $\theta_i = -30°$.

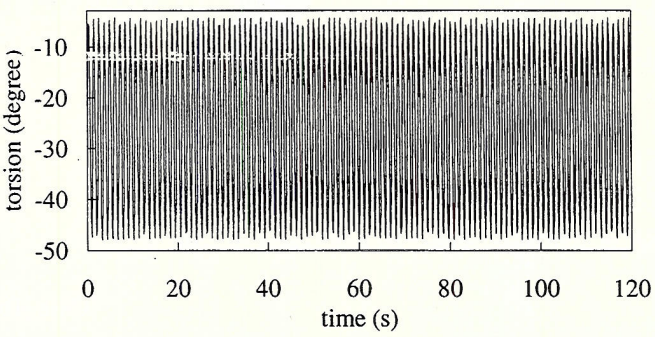

Fig. 13. Torsional displacement, $U_0 = 9.7$ m/s, $\theta_i = -30°$.

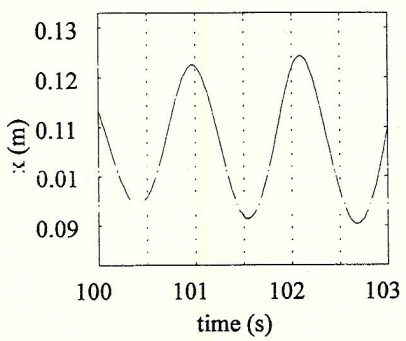

Fig. 14. Horizontal displacement, $U_0 = 9.7$ m/s, $\theta_i = -30°$.

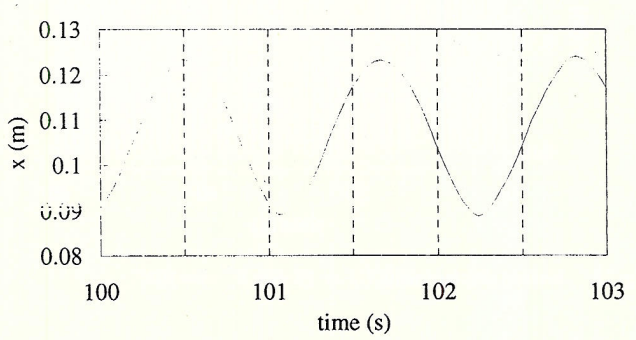

Fig. 15. Horizontal displacement, $U_0 = 9.7$ m/s, $\theta_i = -30°$.

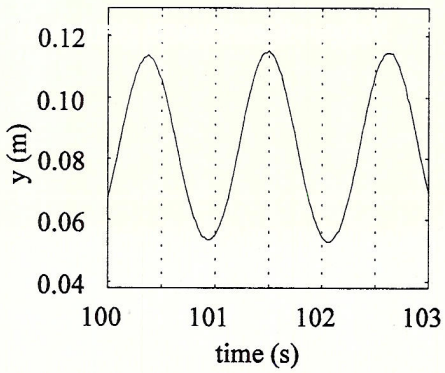

Fig. 16. Vertical displacement, $U_0 = 9.7$ m/s, $\theta_i = -30°$.

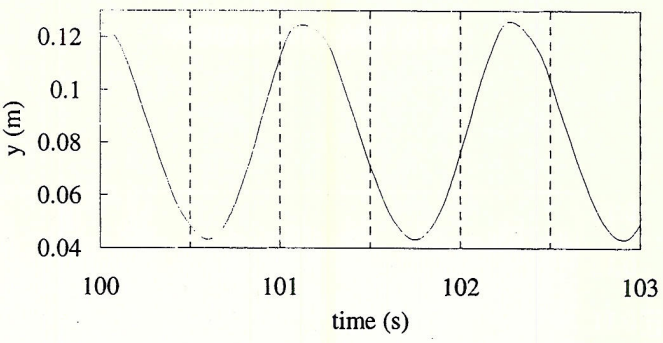

Fig. 17. Vertical displacement, $U_0 = 9.7$ m/s, $\theta_i = -30°$.

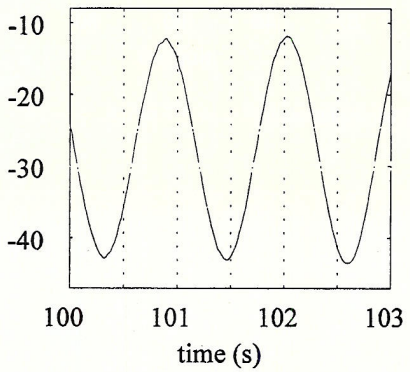

Fig. 18. Torsional displacement, $U_0 = 9.7$ m/s, $\theta_i = -30°$.

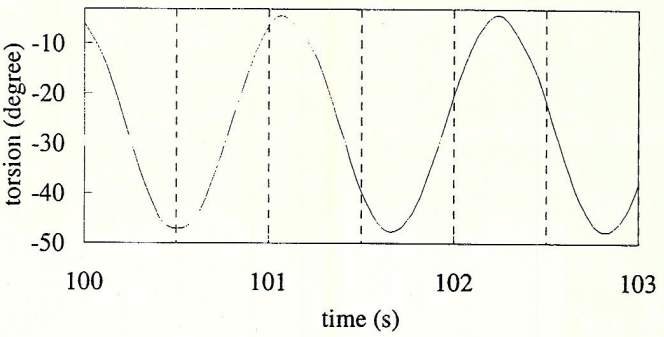

Fig. 19. Torsional displacement, $U_0 = 9.7$ m/s, $\theta_i = -30°$.

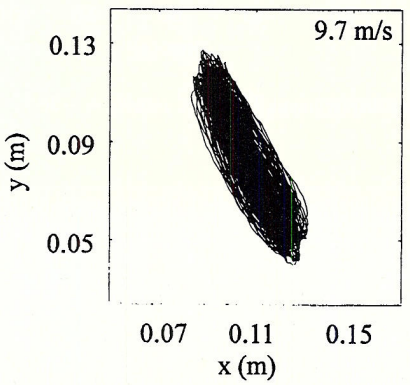

Fig. 20. Galloping "ellipse," $U_0 = 9.7$ m/s, $\theta_i = -30°$.

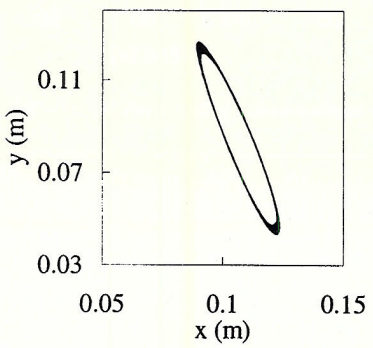

Fig. 21. Galloping "ellipse," $U_0 = 9.7$ m/s, $\theta_i = -30°$.

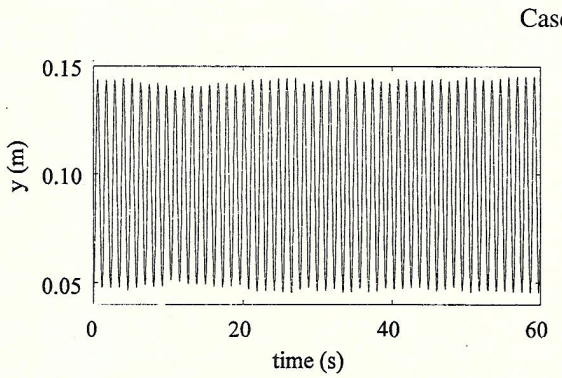

Fig. 22. Vertical displacement, $U_0 = 12$ m/s, $\theta_i = -165°$.

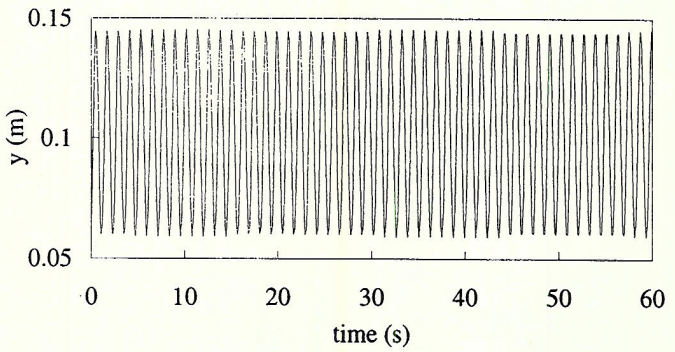

Fig. 23. Vertical displacement, $U_0 = 12$ m/s, $\theta_i = -165°$.

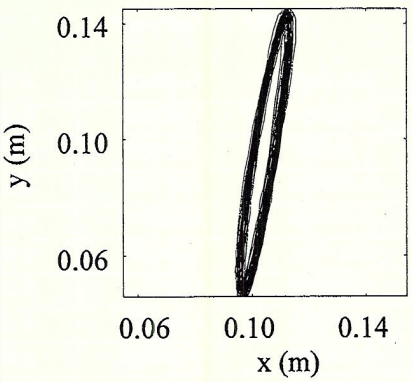

Fig. 24. Galloping "ellipse," $U_0 = 12$ m/s, $\theta_i = -165°$.

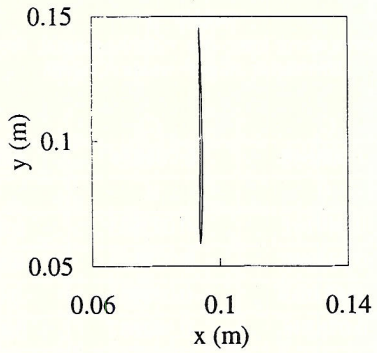

Fig. 25. Galloping "ellipse," $U_0 = 12$ m/s, $\theta_i = -165°$.

Case_2

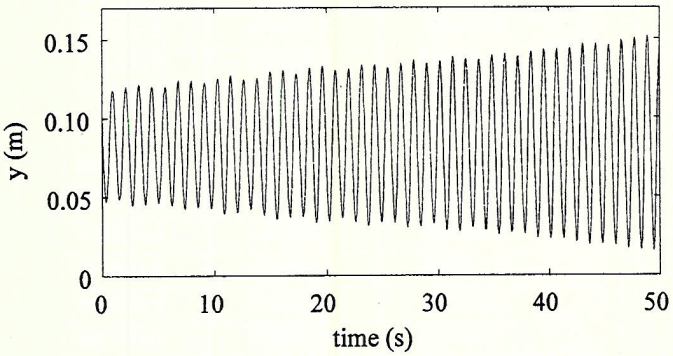

Fig. 26. Vertical displacement, $U_0 = 8.5$ m/s, $\theta_i = -180°$.

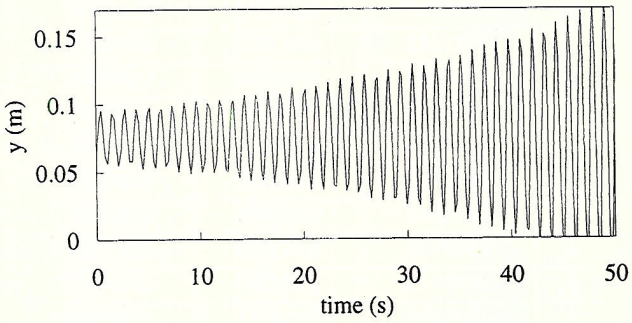

Fig. 27. Vertical displacement, $U_0 = 8.5$ m/s, $\theta_i = -180°$.

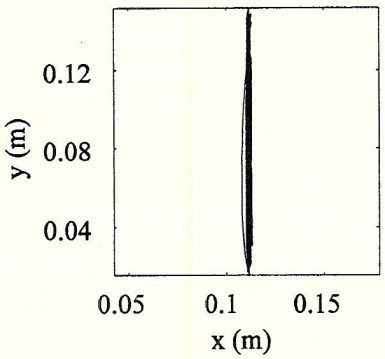

Fig. 28. Galloping "ellipse," $U_0 = 8.5$ m/s, $\theta_i = -180°$.

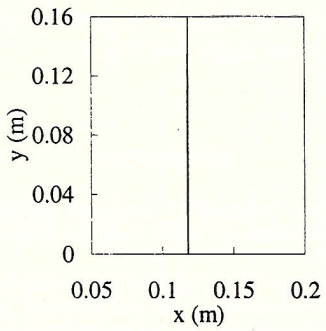

Fig. 29. Galloping "ellipse," $U_0 = 8.5$ m/s, $\theta_i = -180°$.

V. Conclusions

The experimental results presented in this paper are exceptional for several reasons. First they confirm the existence of two kinds of galloping instability mechanisms, namely the flutter galloping instability which is an aeroelastic instability and Den-Hartog's instability which is a pure aerodynamic instability. Second, as the full set of experimental data is known, these results can be used as benchmark cases for the validation of a numerical model for galloping.

Such a validation has been realized in this paper with finite element software. The very good agreement with the simulated results and the experimental ones prove that the quasisteady hypothesis for the action of the aerodynamic forces can be used to forecast the galloping amplitudes with a numerical model.

This latter conclusion is of primary importance because it means that the galloping amplitudes of a real line can be forecast if we have at our disposal quasisteady measured aerodynamic coefficients of the ice shape. It is obvious that the real ice shape is never known *a priori*, but there exists now sufficient wind tunnel measurements of different ice shapes with different eccentricities to simulate most of the natural occurring accretion.

Appendix

The experimental points of the different aerodynamic coefficients (see Fig. 3) are fitted with the following generic formula

$$C_i = \sum_{k=0}^{25} A_k \cos(k(\phi) + B_k \sin(k(\phi))), \quad i = d, l, m$$

TABLE II
FOURIER'S COEFFICIENTS USED FOR THE NUMERICAL FITTING OF THE DIFFERENT AERODYNAMIC CURVES

	C_d	C_l	C_m
A_0	1.308648	0.008854	0.078554
B_0	0	0	0
A_1	0.049181	-0.027835	0.053193
B_1	0.035349	0.023840	0.504328
A_2	-0.623619	-0.038926	-0.010888
B_2	0.078338	-0.362632	0.458776
A_3	-0.152046	-0.073848	0.021819
B_3	0.029337	-0.522246	0.116803
A_4	-0.058744	-0.040637	0.047891
B_4	-0.000927	-0.040174	0.107323
A_5	-0.031866	-0.041813	0.031464
B_5	0.001851	-0.227223	0.114956
A_6	0.013382	-0.025877	0.014113
B_6	-0.003831	-0.028193	0.047891
A_7	0.024382	-0.034643	0.028273
B_7	-0.005716	-0.090097	0.035936
A_8	0.042640	0.002587	0.017275
B_8	-0.012065	0.023618	0.024075
A_9	0.009106	-0.021343	0.017821
B_9	-0.009172	-0.023557	-0.004717
A_{10}	0.012386	0.016753	-0.002250
B_{10}	-0.000350	0.031050	0.000879

where k is the subscript of the Fourier coefficients A_k, B_k which are provided in Table II. In a static configuration the angle ϕ is equal to the angle θ of Fig. 1.

TABLE II (*Continued*)

A_{11}	-0.012692	-0.000483	-0.016334
B_{11}	0.004726	0.007569	0.005758
A_{12}	0.001507	0.004816	0.007732
B_{12}	-0.006914	0.027042	0.010630
A_{13}	-0.011664	-0.004076	0.008188
B_{13}	0.011193	0.004180	0.001315
A_{14}	-0.007597	0.000512	-0.021535
B_{14}	0.005243	0.004142	-0.010036
A_{15}	-0.006958	-0.000262	0.002548
B_{15}	0.003886	0.006142	-0.010977
A_{16}	0.005988	-0.007628	0.009744
B_{16}	-0.003869	-0.003707	0.000693
A_{17}	0.004985	-0.002666	-0.008274
B_{17}	0.004156	0.003093	-0.000199
A_{18}	0.004887	-0.003489	-0.012801
B_{18}	-0.003618	-0.006725	0.004257
A_{19}	0.000737	0.001372	0.006761
B_{19}	-0.005036	0.008182	0.001477
A_{20}	0.002666	-0.006067	-0.005759
B_{20}	-0.005723	-0.001396	0.013766
A_{21}	0.000102	0.003244	0.006753
B_{21}	0.000935	0.004675	-0.004679
A_{22}	0.000174	-0.001315	0.000670
B_{22}	-0.004456	-0.000805	-0.001288
A_{23}	-0.000510	0.002110	-0.006206
B_{23}	0.000457	0.003713	-0.006826
A_{24}	-0.003451	0.000935	-0.002867
B_{24}	0.004797	-0.004871	-0.003511
A_{25}	-0.004310	0.004694	-0.001147
B_{25}	0.003379	0.002193	-0.010406

REFERENCES

[1] C. B. Rawlins, "Analysis of conductor galloping field observations—Single conductors," IEEE Trans. on Power Delivery, Paper no. 81 WM 053-8.

[2] O. Chabart and J. L. Lilien, "Galloping of electrical lines in wind tunnel facilities," in *Proceedings of the 2nd European and African Conference on Wind Engineering*, vol. 2, Genova, Italy, June 22-26, 1997, pp. 1751–1758.

[3] J. P. Den Hartog, "Transmission line vibration due to sleet," *AIEE Trans.*, vol. 51, pp. 1074–1076, 1932.

[4] R. Keutgen and J. L. Lilien, "A new damper to solve galloping on bundled lines. Theoretical background, laboratory and field results," *IEEE Trans. on Power Delivery*, vol. 13, no. 1, pp. 260–265, Jan. 1998.

[5] M. Tunstall and L. T. Koutselos, "Further studies of the galloping instability & natural ice accretion on overhead line conductors," in *4th Int. Conf. on Atmospheric Icing of Structures*, Paris, Sept. 1988.

[6] MECANO, *Finite Element Software for Non-Linear Time Analysis*. Liège, Belgium: Samtech.

Renaud Keutgen was born in Liège, Belgium, on October 18, 1971. He received the degree in mechanical engineering from the University of Liège in 1994. He is currently a Ph.D. student at the same University. His research area concerns the study of single and bundled conductors galloping, aid of the finite element method.

Jean-Louis Lilien was born in Liège, Belgium, on May 24, 1953. He received the degree in electrical and mechanical engineering from the University of Liège in 1976. He received the Ph.D. degree from the same University in 1984. He is presently a Professor at the same University, Dept. of Transmission and Distribution of Electrical Energy. His main activity is based on the effects of short-circuit mechanical effects and overhead lines vibrations (galloping). He is the chairman of the CIGRE task force on the effects of short-circuit in substation (belonging to WG 23-11). He is also an expert of the CIGRE task force on galloping (belonging to WG 22-11). He has published more than 60 technical papers and participated in many symposia and international conferences. He received the international prize "George Montefiore" in 1986.